Part I
General Atomic Force Microscopy

Atomic Force Microscopy in Liquid: Biological Applications, First Edition.
Edited by Arturo M. Baró and Ronald G. Reifenberger.

1
AFM: Basic Concepts

Fernando Moreno-Herrero and Julio Gomez-Herrero

1.1
Atomic Force Microscope: Principles

A conceptually new family of microscopes emerged after the invention of the scanning tunneling microscope (STM) by Binnig and Rohrer in 1982 [1]. This family of instruments called scanning probe microscopes (SPMs) is based on the strong distance-dependent interaction between a sharp probe or tip and a sample. The atomic force microscope therefore uses the force existing between the probe and the sample to build an image of an object [2, 3]. AFMs can operate in almost any environment including aqueous solution, and that opened myriad uses in biology [4, 5]. When thinking about how an AFM works, all notions of conventional microscope design need to be disregarded, since there are no lenses through which the operator looks at the sample. In AFM, images are obtained by sensing with the probe rather than by seeing.

The central part of an AFM is therefore the tip that literally feels the sample. A nanometer-sharp AFM tip made by microfabricating technology is grown at the free end of a flexible cantilever that is used as the transductor of the interaction between the tip and sample. The reflection of a laser beam focused at the back side of the cantilever is frequently used by most AFMs to amplify and measure the movement of the cantilever, although other detection methods may also be used (Section 1.4). The reflected beam is directed to a photodiode that provides a voltage depending on the position of the laser beam. For imaging, the tip is scanned over the sample, or as in some designs, it is the sample that moves with respect to the fixed tip, which is only allowed to move in the vertical direction. In both cases, the fine movements of the tip and sample are provided by piezoelectric materials that can move with subnanometer precision. At each position, the cantilever deflection is measured, from which a topography map can be constructed. This scanning technique in which the tip is brought into mechanical contact with the sample surface is known as *contact mode*, and it was first described by Binnig and coworkers [2]. Both the tip and scanner are the key features in any AFM setup.

Atomic Force Microscopy in Liquid: Biological Applications, First Edition.
Edited by Arturo M. Baró and Ronald G. Reifenberger.

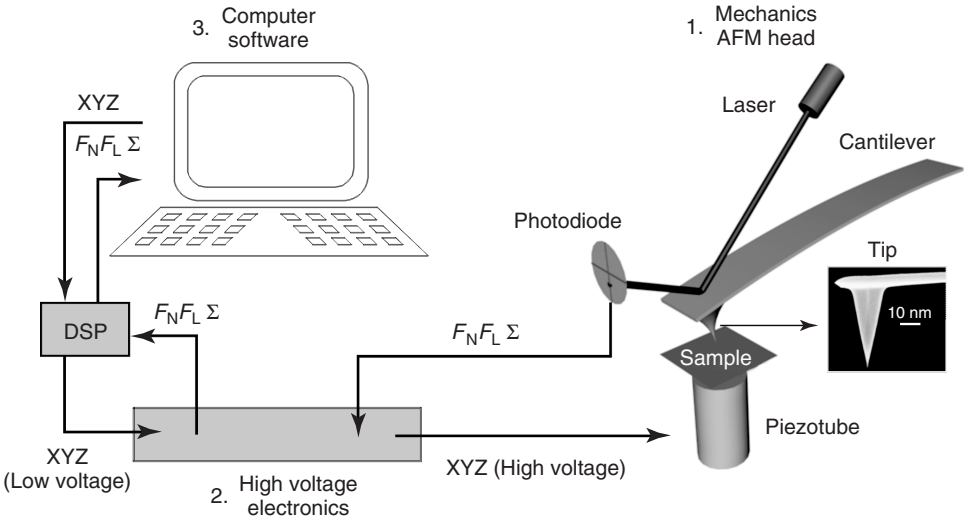

Figure 1.1 Components of a standard atomic force microscope. 1. The AFM head and the piezoelectric stage. The cantilever and its detection system as well as the sample movement are the main parts of this component. From the photodiode, the signals related to the normal and lateral forces (F_N and F_L) as well as the total intensity of light (Σ) are obtained and transferred to the high voltage electronics. 2. The high voltage electronics. This component amplifies voltages from the digital signal processor to perform the movement of the piezotube (XYZ voltages). It also collects signals from the photodiode (F_N, F_L, and Σ) and transfers them to the DSP. 3. The computer, DSP, and software that controls the AFM setup.

One of the most common models of AFM is schematically depicted in Figure 1.1. In this model, the sample is scanned over the tip, but the opposite is also possible. The latter are the so-called stand-alone AFMs that are commonly used combined with an inverted optical microscope to image biological samples in liquid. In either case, a standard AFM setup consists of three main components. (i) *the AFM head and base stage*: The AFM head contains the tip holder, the laser, and the photodiode. It also includes positioning mechanisms for focusing the laser beam on the back side of the cantilever and photodiode and small electronics for processing the signals coming from the photodiode. From this, the vertical (F_N) and lateral (F_L) deflections of the laser beam and its total intensity (Σ) are obtained. The AFM head is placed over a base stage that holds the piezoelectric scanner that moves the sample, and also a coarse, micrometer-ranged approaching mechanism, usually based on step motors.[1)] (ii) *The high voltage (HV) electronics*: It amplifies the signals coming from the digital signal processor (DSP) (XYZ low voltage) to drive the piezoelectric scanner with voltages of about 100 V (XYZ HV). The electronics also transfers the analog voltage signals from the photodiode (F_N, F_L, Σ)

1) On a stand-alone AFM, the tip is scanned over the sample and the approaching mechanisms (step motors) are placed on the AFM head rather than on the mechanical stage.

to the DSP. The HV electronics must be able to amplify small signals from the computer (of some volts) to hundreds of volts needed to move the piezoelectric tube over micrometer distances. It is therefore essential that this amplification does not introduce electrical noises that may affect the resolution of the AFM. (iii) *The DSP, the computer, and the software*: The DSP performs all the signal processing and calculations involved in the real-time operation of the AFM. The DSP is mainly located in a board plugged in the computer. It contains the chips to perform the translation from digital to analog signals (digital to analog converters (DACs)), which are further managed by the HV electronics. Analog signals from the HV amplifier are converted to digital signals also at the DSP board using analog to digital converters (ADCs). Finally, all computer-based systems need software to run the setup. Nearly all AFMs in the market come with purpose-made acquisition software. Raw images can later be processed with any of the many imaging-processing freeware available in the Internet.

Operating the AFM in liquid conditions requires modifications of some parts to prevent wetting of electrical components such as piezoelectric ceramics. For instance, the sample holder must be large enough to accommodate the sample and the buffer in which it is immersed. Some authors simply use a small droplet of some tens of microliters, which covers the sample; others use a small container filled with several milliliters of buffer. The first approach has the advantage of a smaller mass (droplet) added to the piezo, but experiments suffer from evaporation, which results in a change in the concentration of solvents. On the other hand, using the container approach, concentrations are kept roughly constant, but a considerable mass must be moved by the piezo scanner, which reduces its resonance frequency and therefore the range of imaging speeds. The tip holder, also known as *liquid cell* (Section 1.4.2.1), must be designed to prevent contact between the liquid and the small piezo that drives movement of the cantilever. Finally, in some AFMs, the piezo tube is protected and covered to prevent wetting in case of liquid spill (Section 1.2.1).

1.2 Piezoelectric Scanners

Piezoelectric ceramic transducers are used to accurately position the tip and sample in AFMs. The direct piezoelectric effect consists of the generation of a potential difference across the opposite faces of certain nonconductive crystals as a result of the application of stress. The reverse piezoelectric effect is also possible because of a change in dimensions of the crystal as a consequence of the application of a potential difference between two faces of the piezoelectric material. This method is used to position the tip and sample with respect to each other with subnanometer precision since piezoelectric ceramic transducers are highly sensitive, stable, and reliable. Regardless, if the tip is moved over the sample or vice versa, the scan in AFM is performed using piezoelectric transducers.

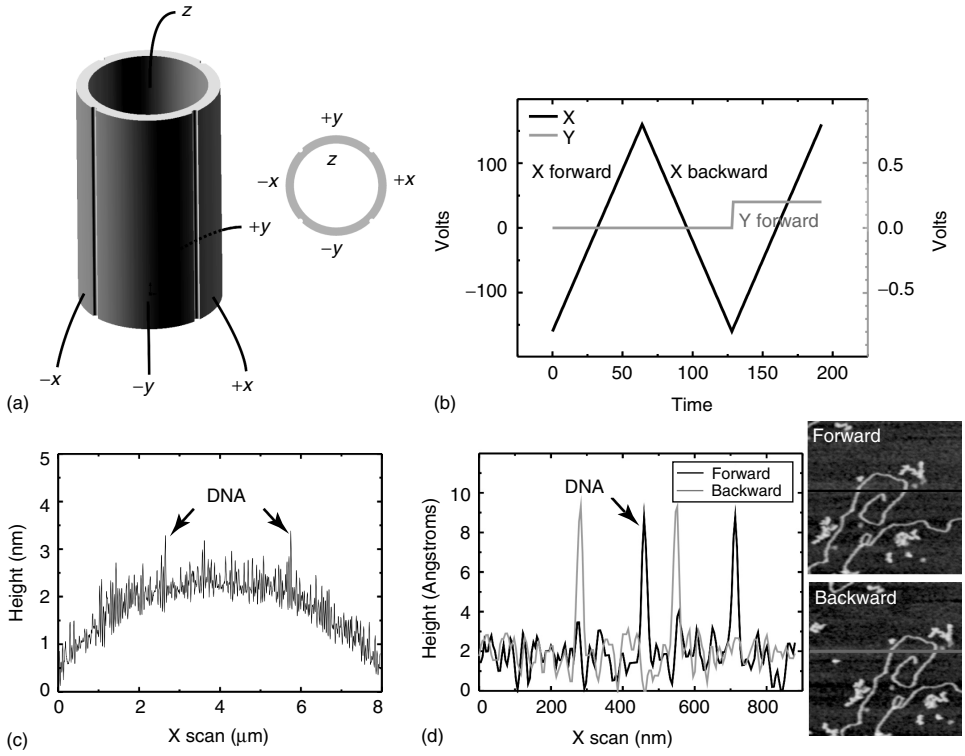

Figure 1.2 Piezoelectric scanners. (a) Piezotube architecture based on four sectors. Voltages are applied between opposite sides, and as a consequence, movement of the piezo is generated. (b) Sequence of voltages applied to X (fast scan) and Y (slow scan) to generate an image scan. Each step in *y*-axis is associated with the change of an imaging line. (c,d)Two typical problems of piezotube scanners. (c) The plane where the sample is situated describes an arc rather than a straight line. (d) Clear effect of piezo hysteresis when imaging DNA molecules.

Many AFMs use piezoelectric tube scanners such as the one shown in Figure 1.2a. They consist of a thin-walled hard piezoelectric ceramic, which is polarized radially [6]. The external face of the tube is divided into four longitudinal segments of equal size and electrodes are welded to the internal and external faces of the tube. To achieve extension or contraction, a bias voltage is applied between the inner and all the outer electrodes. The scan movement is performed by applying a bias voltage to one of the segments of the outer wall. To amplify this bending effect by a factor of two, a voltage with opposite sign is applied to the opposite segment. With a correct synchronization of applied voltages ($\pm x$ and $\pm y$), a sequential scan can be generated (Figure 1.2b). Typically, tube scanners of 10×10 μm range have sensitivities of ∼40 nm/V. This means that voltages up to ±125 V must be generated with submilivolts precision to achieve a basal noise of ∼0.01 nm. This operation is performed by the HV electronics.

Tube scanners have some drawbacks. For instance, the plane in which the sample is located describes an arc rather than a straight line. This effect is more pronounced when large areas are scanned and the height of the objects to be imaged is small compared to the scan area. For instance, Figure 1.2c shows a profile of a flat surface with adsorbed DNA molecules. The effect of the arc trajectory described by the piezo is clearly visible, and the detection of small molecules such as DNA (height < 1 nm) is challenging. This effect can easily be corrected by subtracting a polynomial function to each scan line or to the overall surface. Piezo tubes have relatively low resonance frequencies, of the order of kilohertz, which limits the scan speed. Recently, some manufacturers have employed small stacks of piezoelectric ceramics to increase the resonance frequency of these devices and therefore the imaging speed. However, stacked piezos have a quite limited scan range.

A different approach used to move the sample is based on stick-slip motion. These positioners rely on the controllable use of the inertia of a sliding block. In brief, a sliding block slips along a guided rod, which is otherwise clamped in frictional engagement. A net step is obtained by first accelerating very rapidly the guiding rod over a short period (typically microseconds) so that the inertia of the sliding block overcomes the friction. The sliding block disengages from the accelerated rod and remains nearly nondisplaced. Then, the guiding rod moves back to its initial position slowly enough so that the sliding block sticks to it and thus makes a net step. Periodic repetition of this sequence leads to a step-by-step motion of the sliding block in one direction. The movement of the guiding rod is performed by a piezoelectric ceramic, which can pull or push as required. Stick-slip positioners have long travel ranges of several millimeters, but their performance is dependent on the mass to be moved, which can be significant in liquid imaging. These devices also have the limitation of a relatively large step (few nanometers) and a low resonance frequency (much lower than that of stacked piezos). Hence the main use of these devices is as nanopositioners rather than as fast scanners.

Piezoelectric scanners are inherently nonlinear, and this nonlinearity becomes quite significant at large scans. Typical piezos suffer from hysteresis in the forward and backward traces. This effect can be clearly seen in the forward and backward profiles shown in Figure 1.2d. Piezo scanners are also subjected to creep after changing the polarity (direction) of the scan or just after setting the voltage to zero. This is due to some sort of relaxation, which occurs under constant stress. It has an effect on the images distorting the dimensions of the objects to be imaged. In general, this problem can be solved by repeating the scan, allowing the piezo to relax. To minimize unwanted motions in the piezoactuator, some AFMs incorporate a combination of piezoactuators and metal springs. These devices have flexure-guided stages, acting as springs and restricted to move only in one direction. A piezoactuator pulls against the spring, and therefore a forward and backward movement of the flexure guide can be achieved by changing the voltage in the piezoactuator. This combination effectively decouples the unwanted motions in the piezoactuator and produces a pure linear translation while keeping high resonance frequencies at relatively high loads ($\sim$2 kHz for a 100 g load). Finally, many AFMs

have capacitive sensors incorporated in their piezos that allow for measuring the position independent of the applied voltage. With this feature, a closed-loop circuit can be designed, being able to cancel any hysteresis, creep, or nonlinearity by applying additional correction voltages.

1.2.1 Piezoelectric Scanners for Imaging in Liquids

In many AFMs, the piezoelectric used to image in air is the same as that used to image in liquids, but some precautions must be taken. The main concern is related to the electrical isolation of the piezo to avoid any shortcut due to wetting. HVs (hundreds of volts) are applied to the piezo, and if any water gets into it, the expensive piezo tube will almost certainly be destroyed. Therefore, some caution must be taken when imaging in liquids to avoid any spill of water into the piezo. In most AFMs, some silicone or rubber is added to prevent any liquid from getting into the piezo.

For imaging in liquids, it is often recommended to move the tip relative to the sample instead of keeping the tip fixed and move the sample. In the latter scenario, volumes of milliliters should be moved at kilohertz frequencies, affecting the mechanical stability of the piezo. This is equivalent to considering an effective mass in Eq. (1.3). That will lower the piezo resonant frequency and will slow down the imaging speed of the AFM. Instead, when moving the tip relative to the sample in liquids, the added effective mass is small because only the tip and parts of the tip holder are immersed in the buffer container. When imaging in environments with large viscosity such as liquids, it is important to keep the mass of moving objects as low as possible. This is also important for oscillating the tip; a need in dynamic modes. Some users oscillate the complete tip holder, exciting many mechanical vibrations in the buffer container, which hide the genuine mechanical resonance of the cantilever (Section 1.5.3.1).

1.3 Tips and Cantilevers

In contact mode, to be able to feel the surface with atom resolution, the stiffness of an AFM cantilever should be much smaller than the spring constant that maintains the atoms confined together on the surface. This bonding force constant in a crystalline lattice is of the order of 1 N m^{-1} [7], meaning that to use the AFM in contact mode (Section 1.5.1), the spring constant of the cantilevers (k) should be much smaller than 1 N m^{-1}. To achieve this value of k, a beamlike cantilever made of silicon or silicon nitride should have micrometer dimensions if one considers the formula for the spring constant of a cantilever

$$k = \frac{Et^3 w}{4l^3} \tag{1.1}$$

where E is the Young's modulus of the material (i.e., for silicon nitride $E = 1.5 \times 10^{11}$ N m^{-2}) and t, w, and l are the thickness, width, and length of the cantilever, respectively. For example, a silicon nitride cantilever of dimensions $(t, w, l) = (0.3, 10, 100)$ μm will yield a value of k of 0.01 N m^{-1}, well below the spring constant of the atoms in a crystalline lattice. In principle, one could think that it may be advantageous for imaging soft materials such as proteins to fabricate cantilevers with an arbitrarily low constant. However, there is a fundamental limitation for lowering k. A cantilever in thermodynamic equilibrium with a thermal bath at temperature T has a thermal energy k_BT, k_B being the Boltzmann's constant. Considering the cantilever as a system with just one degree of freedom (it can move only up and down), the thermal energy increases the elastic energy stored in the cantilever as

$$\frac{1}{2}kA^2 = \frac{1}{2}k_B T;\ A = \sqrt{\frac{k_B T}{k}} \tag{1.2}$$

where A is the oscillation amplitude of the cantilever. For a cantilever with $k = 0.1$ N m^{-1}, the thermal noise amplitude is $A \sim 0.2$ nm, a value similar to the atomic corrugation of a surface.

$$f = \frac{1}{2\pi}\sqrt{\frac{k}{m}} = \frac{1}{4\pi}\frac{t}{l^2}\sqrt{\frac{E}{\rho}} \tag{1.3}$$

Equation (1.3) combines the resonance frequency of a harmonic oscillator with the stiffness values of a cantilever. It should be noted that Eq. (1.3) is only exact for a point mass particle, but it is generally considered a good approximation for a continuum mass such as a cantilever. A cantilever of the abovementioned dimensions will have a mass of ∼1 ng (considering a density of 3.44 g cm^{-3} and not taking into account the mass of the tip) and a resonant frequency of approximately few kilohertz, well above the mechanical resonances of the building, for instance. The resonant frequency of the cantilever has important implications related to the imaging speed of the AFM. Let us assume a surface with a corrugation that can be approximated to a sinusoidal function with a wavelength of 2 nm. This means that the cantilever should move up and down at a frequency of ∼5 kHz when imaging a surface of size 10 μm × 10 μm at a speed of 1 line per second (a typical value for AFM). In other words, a wavelength translates to a time period when the cantilever scans the surface at a given speed. In order to respond to such a corrugation, the resonance frequency of the cantilever should be well above the frequency associated with the corrugation. Therefore, it turns out that the use of cantilevers with high resonant frequencies and low stiffness is highly advantageous for fast imaging of soft materials.

The offer provided by several manufacturers of different tips, cantilevers, and materials is very extensive. This large offer has opened the AFM field to multiple applications, such as noncontact AFM (NC-AFM) and dynamic modes, conductive AFM, electrostatic AFM, and so on, and has also given the possibility to image in different environments. The criterion to choose the most appropriate tip and cantilever depends on the application. In general, soft cantilevers are used in contact mode to avoid damage to the sample. On the other hand, stiff cantilevers

Table 1.1 Standard properties of cantilever used for each imaging mode and for liquids and air.[a]

Imaging mode (environment)	K (N m^{-1})	f (kHz) (in air)	Notes
Contact mode (*air* and *liquids*)	<1	10–30	Major requirement is to use soft cantilevers V-shaped cantilevers are preferred to minimize lateral bending Rectangular cantilever are used to measure friction
Jumping/pulsed mode (*air*)	1.5–3	25–70	Requires relatively large K values to overcome capillary and adhesion forces
Jumping/pulsed mode (*liquids*)	<0.1	20	Absence of capillary and low adhesion forces enable use of softer cantilevers than in air
Dynamic modes (*air*)	15–60	130–350	Stiff lever required to give a high Q factor and to overcome capillary adhesion between tip–surface if working in air Moderate amplitude oscillation (>5 nm)
Dynamic modes (*liquids*)	<0.1	30–50	Rectangular or V shape Requires a Q-value over 1 (long tips ~10 μm) Small amplitude oscillation (<5 nm)

[a] Data extracted from manufacturers: Nanosensors and Olympus. *www.nanosensors.com and http://probe.olympus-global.com/en/*.

are preferred for imaging in dynamic mode to overcome capillary forces. Ideally, cantilevers of high resonant frequency and low spring constant are preferred, but this is only possible by reducing the cantilever dimensions, which turns out to be complicated. However, recently, some manufacturers have presented new small cantilevers that are meant to meet the expectations of demanding users. Table 1.1 gives an overview of cantilever properties and their uses in the different imaging modes (see Section 1.5 for reference to imaging modes).

1.3.1 Cantilever Calibration

For some quantitative AFM applications, for instance, force–distance spectroscopy, the spring constant of the cantilever must be precisely determined since the quoted value provided by the manufacturer is only an approximation based on the dimensions of the cantilevers. In some cases, the spring constant of the cantilever can be over 20% off from the quoted value.

Equation (1.3) can be used to calculate the cantilever spring constant if its mass is known. However, the AFM cantilever beam is not a simple point mass added at the end of a spring but has its weight distributed along its length, so Eq. (1.3) is usually modified by considering an effective mass, m_0. In any case, measuring the effective mass of a cantilever is rather complicated, and Cleveland and coworkers [8] proposed a method based on measuring the changes in resonant frequency, f, as small masses, m^*, were added to the cantilever (Eq. (1.4)).

$$\omega^2 = \frac{k}{m^* + m_0} \quad \text{and} \quad f = \frac{\omega}{2\pi} \tag{1.4}$$

A plot of added mass, m^*, versus ω^{-2} has a slope equal to k, and an intercept equal to the effective cantilever mass m_0. By carefully performing the measurements described in [8], Cleveland and coworkers derived the following equation, which allows calculation of k with reasonable accuracy by just measuring the unloaded resonant frequency of the cantilever, assuming that one has accurate information on the length and the width of the cantilever.

$$k = 2w(\pi lf)^3\sqrt{\frac{\rho^3}{E}} \tag{1.5}$$

where l is the length of the cantilever, w its width, ρ is the density of the material, E the elastic modulus or Young's modulus, and f the measured resonant frequency.

A more accurate method was proposed in 1995 by Sader *et al.* [9], and it was improved and applied to rectangular cantilevers in 1999 [10]. This method required to know the width and length of the cantilever, the experimentally measured resonant frequency and quality factor of the cantilever, and the density and viscosity of the fluid (properties of air: density $\rho_{\text{air}} = 1.18\,\text{kg}\,\text{m}^{-3}$ and viscosity $\eta_{\text{air}} = 1.86 \times 10^{-5}\,\text{kg}\,\text{m}^{-1}\,\text{s}^{-1}$). Sader's method was extended to enable simultaneous calibration of the torsional spring constant of rectangular cantilevers in 2004 [11]. The advantages of these methods are that the thickness, density, and resonant frequency in vacuum of the cantilever are not needed. In addition, they are rapid to use, simple to implement experimentally, noninvasive, and nondestructive (*http://www.ampc.ms.unimelb.edu.au/afm/calibration.html*).

1.3.2
Tips and Cantilevers for Imaging in Liquids

In solution, the charge of an object (i.e., of the tip and cantilever) is normally screened by mobile ions in the surrounding electrolyte. Coions (ions with the same sign of charge) are repelled from the surroundings of the object. Counterions (ions with opposite charge) are electrostatically attracted to the object, but this attraction diminishes their entropy. Their spatial distribution is a compromise between these two opposite tendencies. The resulting arrangement of screening charges around the object is known as the *electric double layer*, and its structure has a major impact on interactions between charged objects in solution [12]. Therefore, in contrast to air imaging, where capillary forces play a central role in the tip–surface interaction, in liquid imaging, electrostatic interactions are the most relevant ones. This means

that resolution, which is closely related to tip–sample distance, depends on the arrangement and screening of charges in solution, and therefore, high resolution in buffer can only be achieved if contact takes place between the tip and sample. The fact that imaging in buffer at high resolution requires contact is a major issue when imaging soft samples because soft cantilevers are needed. Originally, soft cantilevers could only be used in contact mode because of their low resonant frequency. Imaging in contact mode implies the presence of shear and lateral forces that could damage soft samples or drag objects along the surface. This problem was partially overcome with the use of pulsed modes such as jumping mode, pulsed force mode, or force volume mode that minimized lateral forces. Recently, some cantilever manufacturers have developed cantilevers designed for imaging soft samples in buffer with low spring constants and reasonably high resonant frequencies, thus allowing the use of dynamic modes. This has increased the range of measurements and has minimized shear and lateral forces. However, fine tuning of electrolyte concentrations is still required to minimize the distance of electrostatic interactions between the tip and sample and to achieve high resolution.

Figure 1.3 exemplifies the relevance of proper tuning of the amount of monovalent and divalent ions when operating in liquids. It shows experimental data of force (cantilever deflection) as a function of piezo extension obtained in different liquids using a soft cantilever of 0.08 N m^{-1} and freshly cleaved mica as a surface. The deflection or force is zero until an attractive (negative) force pulls the cantilever toward the mica. Once the cantilever is in contact with the surface, the deflection follows the piezo movement. When using water (black curve), this attractive force is

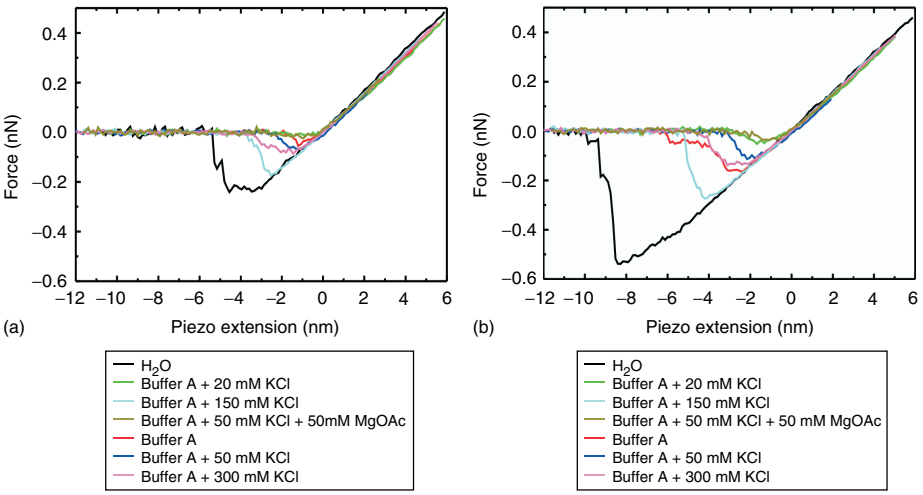

Figure 1.3 Approaching (a) and withdrawing (b) force-extension curves for a mica surface immersed in different buffers. The cantilever used had a force constant of 0.08 Nm^{-1}, and Buffer A is 25 mM tris-acetate pH (7.5) and 2 mM MgOAc supplemented with KCl or extra MgOAc when stated.

over 0.5 nN, a rather large force when imaging biological materials. Data obtained using 25 mM tris-acetate (pH 7.5), 50 mM KCl, 50 mM MgOAc (dark yellow curve) shows an effective absence of adhesion and attractive force.

1.3.3 Cantilever Dynamics in Liquids

According to Eq. (1.1), the spring constant k only depends on the material properties of the cantilever and its geometrical dimensions. This means that k is independent of the surrounding environment in which the cantilever may be immersed. However, viscosity of the surrounding media does affect the mechanical response of the cantilever, and this is important when operating in liquids. Equation (1.3) already indicates that moving the cantilever from air to a more dense fluidlike liquid will have an immediate effect on its resonant frequency, which is reduced because it has to move an extra mass [13]. In addition, the liquid viscosity is much higher than the viscosity of air. The movement of a cantilever driven by an external oscillatory force $F(t) = F_0\cos(\omega t)$ can be described as a forced harmonic oscillator with damping [14].

$$m\ddot{z} + k\dot{z} + \gamma z = F_0\cos(\omega t) \tag{1.6}$$

$$\gamma = \frac{m\omega_0}{Q} \tag{1.7}$$

$$\omega_r = \omega_0\sqrt{\left(1 - \frac{1}{2Q^2}\right)} \tag{1.8}$$

Here, z describes the vertical movement of the cantilever, m is its mass (note that an effective mass m^* can substitute m in all these equations), ω_0 is its free (vacuum) resonant frequency and ω_r its resonance frequency in a fluid, Q is the quality factor, γ the damping coefficient, and F_0 the amplitude of the oscillatory force at a time t.

The solution of Eq. (1.6) has a transient term and a steady term [15].

$$z = B\exp(-\alpha t)\cos(\omega_r t + \beta) + A\cos(\omega t - \varphi) \tag{1.9}$$

The transient term is reduced by a factor of $1/e$, after a time $1/\alpha = 2Q/\omega_0$. From then, the motion of the tip is dominated by the steady term. The steady term is a harmonic function with a phase lag with respect to the external excitation force. Amplitude and phase lag can be calculated with the following equations:

$$A(\omega) = \frac{\frac{F_0}{m}}{\sqrt{\left(\omega_0^2 - \omega^2\right)^2 + \left(\frac{\omega\omega_0}{Q}\right)^2}} \tag{1.10}$$

$$\tan(\varphi) = \frac{\frac{\omega\omega_0}{Q}}{\omega_0^2 - \omega^2} \tag{1.11}$$

Examples of amplitudes and phase lags are shown in Figure 1.4 for different values of Q.

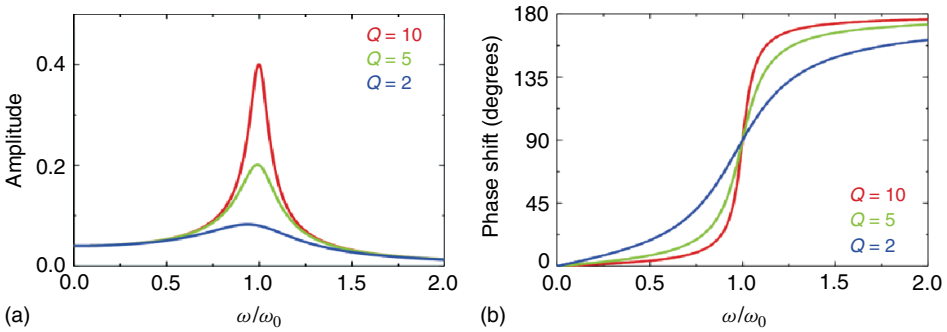

Figure 1.4 Plots of Eqs. (1.9) and (1.10) highlighting the role of the quality factor Q in a harmonic oscillator.

The oscillation of a cantilever in liquid has important differences compared with its oscillation in air or in vacuum. First, as a consequence of the large density of the surrounding liquid compared with the density of air, the cantilever suffers an increase of the effective mass by a factor of 10–40 and a corresponding decrease of the resonant frequency (Eq. (1.3)). Resonance and natural frequencies are related by Eq. (1.8). Therefore as a second consequence, the strong hydrodynamic interaction between the cantilever and the liquid produces a very low quality factor Q. Typically, Q in liquids can be about two orders of magnitude lower than in air (Figure 1.5) [16]. The decrease in resonant frequency and Q has important consequences on the cantilever oscillation and therefore affects the performance of dynamic modes. First, the cantilever oscillation is inharmonic and asymmetric in liquids [17], in contrast with its performance in air where the oscillation is sinusoidal and symmetric [18]. In addition, the low quality factor of the cantilever

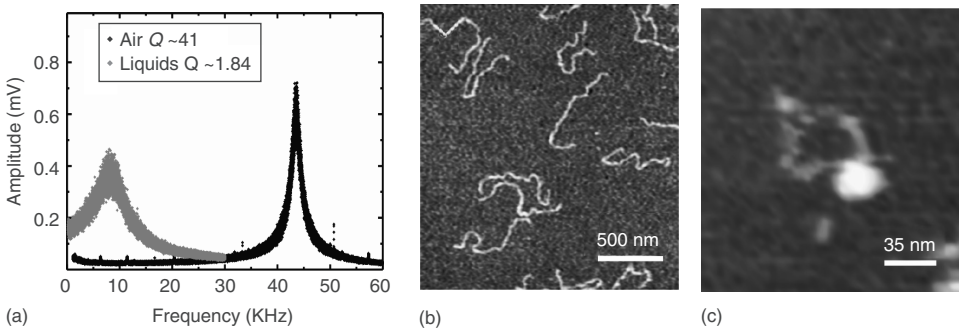

Figure 1.5 (a) Oscillation of the cantilever in air and in liquids. The thermal spectrum of the cantilever (Olympus BL-RC-150VB, $k \sim 0.03$ N m^{-1}) illustrates the reduction in resonant frequency and Q in liquids. (b,c) Examples of images of biomolecules obtained in liquids using dynamic modes and soft cantilevers (Olympus TR400PSA, $k \sim 0.08$ N m^{-1}). (b) DNA molecules imaged in 10 mM tris-HCl (pH 8.0), 5 mM MgCl2. (c) Rad50/Mre11 protein complex in 25 mM tris-HCl (pH 8.0), 125 mM KCl and 10% Glicerol. (a) Adapted from Ref. [19].

in liquid implies high forces between the tip and sample [19]. Dynamic modes use as a control signal, the amplitude of the oscillation that reflects the interaction between the tip and the sample. A shift in the resonant frequency of the cantilever due to tip–sample interaction produces an amplitude damping at resonance, which is proportional to the quality factor of the cantilever. Some authors developed an AFM technique for liquids in which the cantilever response is controlled by adding an active feedback system that increases the quality factor up to three orders of magnitude [16]. Alternatively, use of cantilevers of high resonance frequency in liquids should improve the performance of dynamic modes, although high frequencies are achieved at the expense of increasing the force constant, which is not convenient for imaging soft materials. Although cantilevers of low k and high f are preferable, molecular resolution has been obtained in buffer using cantilevers of $k \sim 0.08$ N m^{-1} and $f \sim 7$ kHz as can be seen in Figure 1.5 [20].

1.4 Force Detection Methods for Imaging in Liquids

The heart of an AFM is a sharp tip that interacts with a force at the surface of a sample. As seen before, the tip is mounted on a flexible beam whose geometrical and material properties makes it possible to probe the force with high sensitivity. The role of the beam is to translate the force acting on the tip into a deflection that can subsequently be monitored by various means. Among these, tunneling of electrons (the original scheme invented by Binnig and coworkers), capacitance, piezoelectric cantilevers and tuning forks, optical interferometry, and optical beam deflection have been developed to a high degree of sophistication. The interaction force is proportional to the deflection of the cantilever following Hooke's law. Electrical methods such as electron tunneling or capacitance were historically the first used to detect the small movement of the cantilever, but they are not applicable to in-liquid imaging. Interferometry has very high sensitivity and signal-to-noise ratio, but the instrument is difficult to set up and gets quickly misaligned. For this reason, it is not used in liquid AFM. For liquid operation, most AFMs use the laser beam deflection method, but piezoelectric cantilevers and tuning forks can also be employed. In the following section, we introduce both methods.

1.4.1 Piezoelectric Cantilevers and Tuning Forks

The piezoelectric cantilever detection method [21] uses a cantilever with an additional piezoelectric thin film containing electrical connections. As the cantilever bends, the piezoelectric layer is stressed and deformed, altering the charge distribution at both sides of the layer (direct piezoelectric effect). By making proper contacts at both sides of the layer and using a simple preamplifier circuit, it is very easy to obtain a voltage proportional to the cantilever deflection (Figure 1.6a). This method has the advantage that the same connections used to detect deflection can be used

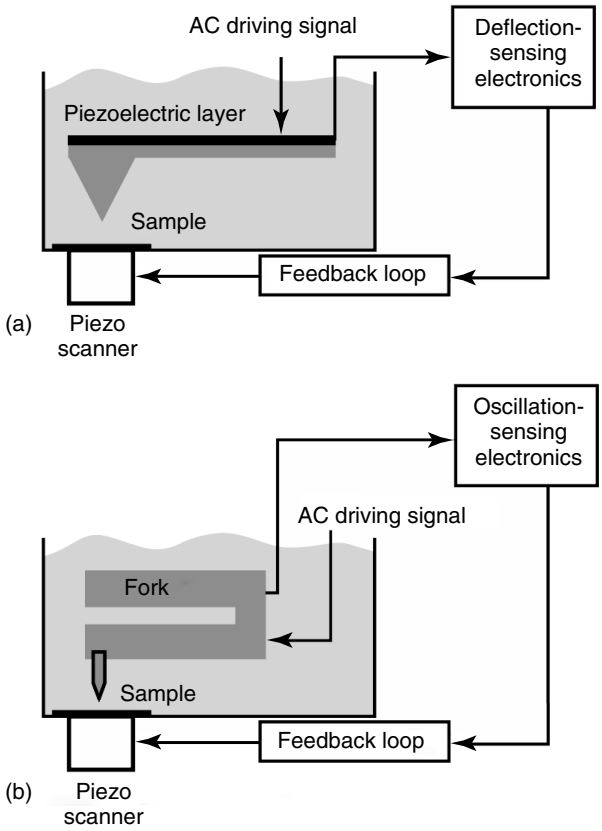

Figure 1.6 (a) Piezoelectric cantilever method and (b) tuning fork method.

to oscillate the cantilever by applying an AC voltage to the piezoelectric film. Piezoelectric cantilevers are also convenient for dynamic operation in liquids. When a cantilever is oscillated in liquid using acoustic excitation, a number of spurious resonances, which are related to the mechanics of the experimental setup, make it very difficult to identify the true cantilever resonant frequency (see discussion in Section 1.5.3.1). In the case of self-oscillated cantilevers, since the only moving object is the cantilever itself, the response of the system does not exhibit the spurious peaks associated with an external drive [22]. On the other hand, electrical contacts in liquids are tricky and may cause unstable oscillation of the cantilever. In addition, this method requires rather expensive cantilevers, often custom manufactured, and their sensitivity is not as good as in optical detection systems.

A similar self-oscillating and detection approach uses a tuning fork for detection of the tip–sample distance (Figure 1.6b). In general, an AFM tip is glued onto one leg of a small quartz tuning fork and it is forced to oscillate. Damping of the amplitude by tip–sample interaction forces is monitored and/or used as a feedback signal. The force resolution of this technique is typically 0.1 pN. This method

is employed for NC-AFM [23] (see dynamic modes, Section 1.5.3) and has the advantage that the probe does not touch the sample surface, and therefore damage to the sample by the probe can be avoided. However, many problems must be overcome for the successful application of NC-AFM to biomaterials or biosystems. First, the large oscillation amplitude of the order of 10 or 100 Å used to attain a sufficient signal-to-noise ratio makes interpretation of the force curve difficult. This problem can be solved by using a stiffer force sensor compared to the conventional ones. Second, in liquids, sufficient Q-value required for NC-AFM measurement is hardly implemented because of the viscosity of the liquid.

1.4.2
Laser Beam Deflection Method

Laser beam deflection is the most common detection method used in modern commercial AFMs and was pioneered by Meyer and Amer [24, 25]. The cartoon in Figure 1.7a describes its functioning principle. The cantilever deflection is measured by monitoring the position of a laser beam reflecting from the cantilever and directed to a quadrant photodiode. The photodiode is a semiconductor device that turns the intensity of light falling on it into an electrical voltage signal. The photodiode is usually split into four sections, enabling both vertical and lateral movements of the cantilever to be differentiated. Vertical movement of the cantilever is measured as the difference in voltage between upper and lower quadrants of the photodiode. Similarly, torsional motion of the cantilever is measured as the difference in voltage between the left and right quadrants of

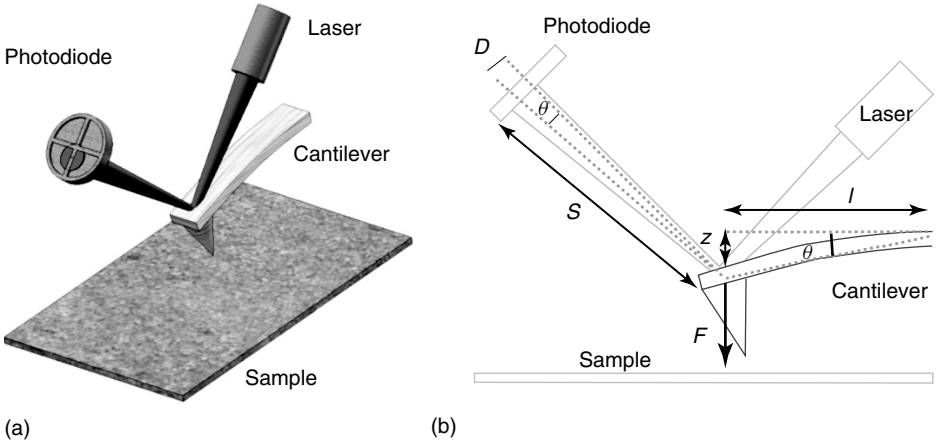

Figure 1.7 Beam deflection method. (a) Cartoon showing the principle of the beam deflection method. A laser beam is focused on the back side of the cantilever and its reflection is directed to a photodiode that records the vertical and lateral movements of the cantilever. (b) A side view of the setup with the relevant dimensions.

the photodiode. Vertical movement of the cantilever originates from the so-called normal forces. The origin of torsional movement of the cantilever arises from frictional forces that originate by the lateral motion of the tip with respect to the sample during the scan [26]. The accuracy of the beam deflection method can be as high as 0.1 Å and is generally limited by random thermal excitation of the cantilever on which the tip is mounted.

It can be shown that the angle at the end of a lever in the presence of a force F acting at this point is [27] (Figure 1.7b)

$$\theta = \frac{Fl^2}{2EI} \tag{1.12}$$

where E is the Young's Modulus and I the area moment of inertia. For a rectangular cantilever, $EI = kl^3/3$, where k is the spring constant fulfilling $F = kz$ and l is the cantilever length. Then we get

$$\theta = \frac{3}{2}\frac{z}{l} \tag{1.13}$$

And since for small deflections $\tan\theta \sim \theta$ and $\tan\theta = D/S$

$$D = \frac{3}{2}\frac{S}{l}z \tag{1.14}$$

This is a large amplification of the movement because for a cantilever of $l \sim 200$ µm at a distance $S \sim 5$ cm, this method amplifies the movement of the cantilever by a factor of 375. In general, the beam deflection method is less sensitive than other electronic methods, but the simplicity of the implementation makes it the preferred method to detect the cantilever deflection in air and in liquids.

1.4.2.1 Liquid Cells and Beam Deflection

The experimental device that allows the laser beam to propagate without suffering scattering in the liquid surface is known as *liquid cell*. The importance of this device is illustrated in Figure 1.8. In almost any air–liquid interface, small mechanical instabilities give rise to surface waves in the liquid that scatter the light coming from a laser beam, producing a noisy spot that is useless for detecting the cantilever deflection (Figure 1.8, left). This problem is solved by creating a well-defined solid–liquid interface with a transparent window. The incoming laser beam (right red line) is transmitted in the liquid without being affected by any surface wave, resulting in a stable spot suitable for detecting the cantilever deflection (Figure 1.8, middle).

The degree of sophistication of a liquid cell depends on the imaging mode employed. We discuss later that there are imaging modes in which the cantilever is oscillated at a particular frequency, and that complicates the design of a liquid cell. Precisely, to oscillate a standard cantilever, most liquid cells incorporate a piezoelectric ceramic, which is isolated to prevent wetting. Some liquid cells use magnetic cantilevers and then there is no need for using piezoelectrics since the cantilever oscillation is achieved with an external magnetic field. Often, the liquid has to be changed in the course of an experiment. Some liquid cells incorporate two

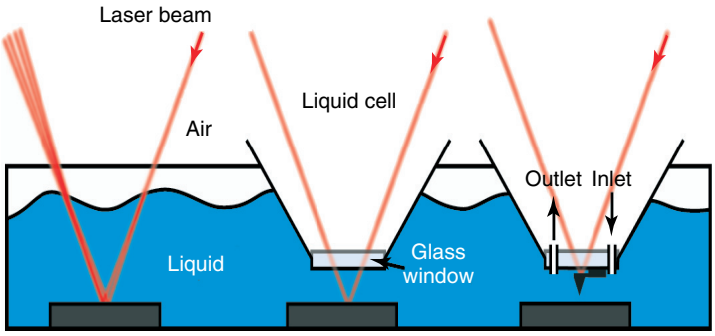

Figure 1.8 Need of a liquid cell device for imaging in liquids. The incoming laser beam (red line) continuously changes direction due to surface waves at the gas–liquid interface. As a consequence, a nonsteady spot is obtained (left). By using a transparent glass window, a well-defined interface is created and the laser light is transmitted without scattering in the liquid (middle). By means of two holes, liquid can be exchanged in the course of an experiment (right).

holes (Figure 1.8, right) at the tip mount. This permits to flow the required solution in and out of the bath, allowing a constant renewal of the liquid environment. The exchange of buffer may cause turbulences in the surrounding of the cantilever. Therefore, to prevent tip damaging, it is recommended to perform this operation with the tip out of contact. Once the old buffer is replaced, the tip can again be approached and set in range for imaging.

1.5 AFM Operation Modes: Contact, Jumping/Pulsed, Dynamic

Imaging modes in AFM are generally classified as static or dynamic modes. This classification is related to the oscillation of the tip during imaging. In static mode, the tip does not oscillate, and in dynamic mode, the tip is forced to oscillate at or near its resonant frequency. Static modes mainly include contact and jumping or pulsed force modes, while dynamic modes include, among others, amplitude-modulation atomic force microscopy (AM-AFM) and frequency-modulation atomic force microscopy (FM-AFM). In the following sections, a general description of the most important ones is given.

1.5.1 Contact Mode

Contact mode atomic force microscopy (CM-AFM) is the oldest and simplest AFM imaging mode in which the tip is brought into direct contact with the surface, deflecting the cantilever (repulsive force) [2]. This deflection is measured in liquid by any of the methods described in Section 1.4 and controlled by a feedback system that keeps it constant. In practice, most AFMs use the beam deflection method,

and therefore, the signal used as control is the one given by the photodiode that corresponds to vertical deflection of the cantilever. The value at which images are taken (usually known as the *feedback set point*) is chosen by the operator depending on the conditions of the experiment. As the tip scans the surface, the Z-scanner is automatically adjusted maintaining the normal signal from the photodiode equal to the set point (see later the feedback loop Section 1.6). First applications of AFM in liquids used this operation mode [5]. AFM was used in contact mode to investigate membrane-bound proteins ordered in 2D arrays [28] and to image the chaperonins GroEL and GroES from *Escherichia coli* [29]. However, these first approaches to AFM in biology soon evidenced that contact mode imaging had several drawbacks. First, the set point given by the operator is related to a certain position of the deflected beam in the photodiode and may not reflect a constant force applied to the sample. This is because the photodiode signal that corresponds to free cantilever deflection (out of contact, zero force) may drift with time. As a consequence, while images are taken at constant deflection, they may not be taken at constant force. Second, the normal force in combination with the lateral motion during scanning introduces high lateral forces (friction) that can damage or move the sample. This is particularly relevant for the case of soft biological materials weakly attached to a surface (DNA, proteins, viruses, etc.). In order to minimize shear forces and to accurately control the force applied while imaging, several methods have been developed, and a brief description is given below.

1.5.2 Jumping and Pulsed Force Mode

Jumping mode atomic force microscopy (JM-AFM) [30] combines features of contact and dynamic modes (Section 1.5.3) and is very similar to pulsed force microscopy [31]. It was originally developed as a scanning mode to minimize shear forces and to accurately control the force applied on an image, while the tip is in contact. In JM-AFM, a force-extension measurement is performed on each of the pixels of the image. JM-AFM mode operation can be described as a cycle repeated at each image point with the following four steps: (1) tip–sample separation (moving from point A to B and C in Figure 1.9), (2) lateral tip motion at the largest tip–sample distance, (3) tip–sample approach (moving from point C to D and A in Figure 1.9), and (4) feedback enabled, which is generally performed on the cantilever deflection (point A in Figure 1.9). From this cycle it is clear that shear forces are minimized because lateral motion is always performed out of contact and that the applied force is controlled because the zero-force level is known and adjusted for each cycle.

JM-AFM solved some of the technical problems occurring in contact mode, for instance, the drift in the zero-force level, but its performance is still seriously affected by the environment used for imaging because of the presence of contact between the tip and sample. In air, the strong adhesion force arising from van der Waals and capillary forces makes it difficult to obtain reproducible images of biomolecules because forces of hundreds of picoNewtons are induced by the mere

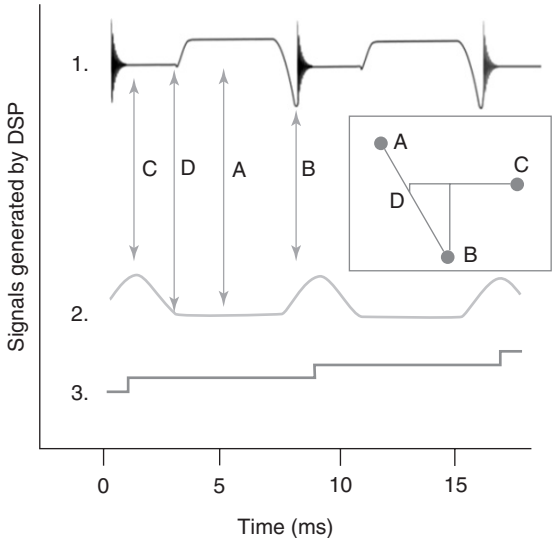

Figure 1.9 Jumping mode oscilloscope signals. (1) Normal force signal or cantilever deflection. (2) Piezoelectric Z (vertical) signal. (3) Piezoelectric (X) lateral displacement as a function of time. In the inset, a force (signal 1) versus extension (signal 2) curve is shown including main points of interest. (A) Region with feedback on. (B) *Jump-off* point or point of maximum negative deflection of the cantilever (adhesion force). (C) Largest tip–sample distance. (D) *Jump-in* point or position where tip–sample contact is established. Adapted from Ref. [30].

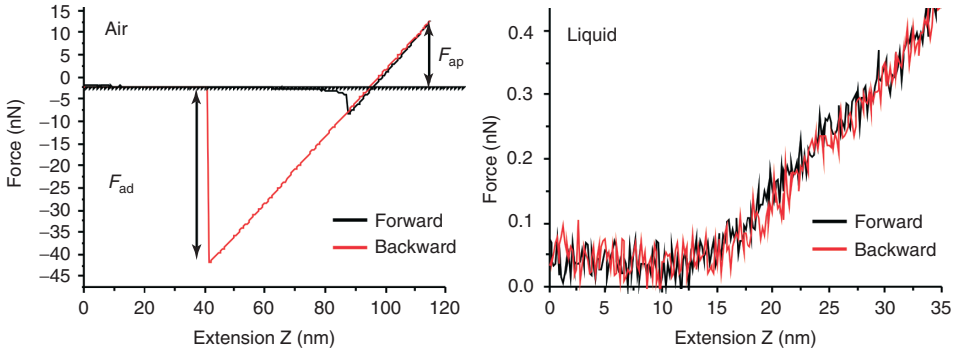

Figure 1.10 Force-extension curves in air and in liquids, enhancing the role of van der Waals and capillary forces in both environments.

contact with the sample (Figure 1.10). In liquids, however, the absence of both capillary forces and low van der Waals forces dramatically decreases the magnitude of the applied forces. This benefits imaging in JM-AFM in liquids, as it has been shown for imaging DNA molecules and viral capsids [17, 32, 33]. Moreover, this method can be used to get information on the mechanical properties of the sample

by performing force-extension curves at each image point. For instance, mechanical properties of virus [33, 34] and unfolding of proteins [35] have been investigated. However, JM-AFM has some drawbacks as, for example, the low imaging rate because of the time consumed during its operating cycle.

1.5.3 Dynamic Modes

The common feature of dynamic modes is that the cantilever is driven at, or close to, its free (far from the surface) resonant frequency f_0. There are two major dynamic AFM modes, AM-AFM and FM-AFM, which are classified according to the signal used as feedback: amplitude and frequency of the oscillating cantilever, respectively. In AM-AFM, the cantilever is excited at $\sim f_0$ with a given oscillation amplitude A_0 (Figure 1.11a,b). Then, the oscillating tip and sample are approached as the amplitude signal is monitored. The amplitude of the cantilever can be measured with a lock-in amplifier or with a much simpler root-mean-square (RMS) detector. At some point, the tip starts *feeling* the interaction with the surface and as a consequence, the amplitude decreases linearly with the distance between the tip and surface. A naive way of surface *feeling* is to imagine the tip to be in intermittent contact with the surface, as if one taps the surface with a finger (Figure 1.11c,d). This is why AM-AFM is usually known as *tapping mode* [36–38]. Generally speaking, the degree of reduction of the amplitude in the tapping region with respect to the free amplitude defines the force applied on the sample and in many occasions, the quality of the image.

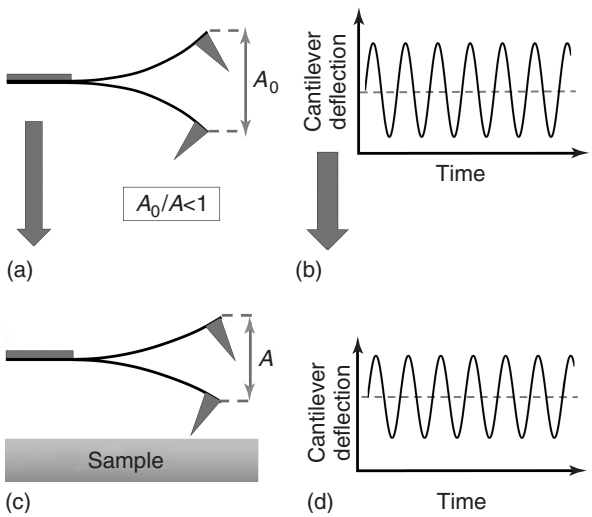

Figure 1.11 Principles of dynamic-mode AFM. (a) Cantilever driven at its free resonance frequency f_0 with amplitude A_0. (b) Rendering of the cantilever deflection as a function of time using, for instance, the beam deflection method. (c) The cantilever is approached to the sample surface and the oscillation amplitude is reduced to A. (d) Same as in (b) but with the cantilever near the surface.

In FM-AFM, the cantilever is kept oscillating with a fixed amplitude at its resonant frequency [39, 40]. An image is formed by scanning at a constant frequency shift (difference between current frequency and the free resonant frequency). FM-AFM is the preferred imaging mode in ultrahigh vacuum (UHV), but recently, true atomic resolution on mica has been reported using this method in liquids [41]. Some authors are now using FM-AFM in liquids as a method to obtain the highest resolution [42].

Despite the superior performance of dynamic modes in air with respect to contact or jumping/pulsed mode, in liquids, both methods yield comparable results. In liquids, van der Waals forces are very weak and there are no capillary forces. As a consequence, in dynamic modes in liquid, contact between tip and sample takes place and forces involved in the working cycle of dynamic and jumping modes are very similar. Nevertheless, there is still an obvious difference between both operating modes, namely, the time consumed in performing each cycle per image point: approximately milliseconds in the case of jumping/pulsed and <0.1 ms in dynamic modes. This affects the imaging rate and gives advantage to dynamic modes compared to others. However, there is still room for improvement because owing to the large effective mass of the cantilever in liquid, its resonant frequency drops and the high damping strongly reduces the Q factor of the system, which in turn means a reduction of the sensitivity of the technique.

1.5.3.1 Liquid Cells and Dynamic Modes

For working in static modes (contact, jumping, or pulse force mode), a liquid cell is almost nothing else but what is shown in Figure 1.8. However, working in liquids in dynamic modes, where the cantilever has to oscillate at or near its resonant frequency, involves a higher degree of sophistication in the liquid cell design. The most common way to oscillate a cantilever in air or vacuum is to use acoustic driving, in which a small piezoelectric element with a very high resonant frequency is located right below the cantilever chip. When working in liquid, this is not so simple because the liquid can easily get in contact with the piezoelectric, creating shortcuts and potential leaks. A simple way to avoid this problem is to locate the small piezo element far away from the liquid. In the liquid cell shown in Figure 1.12, the piezoelectric is located under one of the supporting balls. This solution has an important drawback as the piezo element excites many different mechanical resonances of the liquid cell, thus producing a *forest of resonances*, in which, in many cases, it is almost impossible to locate the real resonance of the cantilever [43]. For amplitude modulation, the right selection of the peak that corresponds to the resonant frequency of the cantilever seems to be not so important, and in many cases, a resonance peak chosen close to the one assumed for the cantilever works fine. For more sophisticated working modes such as frequency modulation a clean resonance and phase lag are required.

There are several remedies for solving the *peak forest* problem. The most common one is to use magnetic driving, in which a coil is placed close to a cantilever covered with a magnetic material (usually cobalt) [44–46]. In this design, the cantilever is driven by a magnetic field induced by an AC current that passes through the coil.

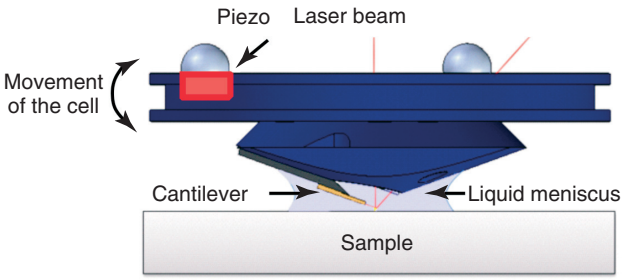

Figure 1.12 Side view of a design of a liquid cell showing a possible mechanism to oscillate the cantilever. A piezoelectric ceramic is located below one of the supporting balls and far away from the liquid meniscus. This solution also moves the liquid, and that excites many other resonances of the liquid cell.

Obviously, this method requires magnetic cantilevers, but the frequency spectrum is free of spurious resonances and the cantilever resonance is very easy to identify. A somewhat similar approximation is the electrostatic excitation, which also requires covering the cantilever with a metal thin film [47]. This method is not as restrictive as the magnetic excitation, but still, not all types of cantilevers can be used. There are also attempts to improve the acoustic driving methods in liquids by moving the piezoelectric closer to the cantilever and selecting a good combination of materials with different impedances. The results are still not as good as in magnetic or electrostatic driving, but cantilevers do not need any special coverage [48, 49]. Recently, a new approach using a secondary laser beam to excite the cantilever has been described [50].

1.6 The Feedback Loop

AFM operation is based on the ability to keep constant a given parameter: deflection, amplitude, phase shift, and so on. This task is done by the AFM control system, which should be as accurate and fast as possible in order to give it a sufficient bandwidth. Control theory provides an extensive arsenal of schemes and procedures to carry out this task. The most common one introduces three mathematical terms to the control signal: proportional (P), integral (I), and differential (D). This control method is commonly known as *PID*. While in early AFM designs, this feedback system was completely analog, the advantages of computer-controlled digital feedback were soon realized, and at present, most SPMs use digitally controlled systems [51]. In most digital controllers, a built-in timer provides the time base for the so-called interruption, which is a piece of code in the control algorithm that is executed at a given frequency. Execution of this code ensures a well-defined and consistent timing (dt) for the control subroutines. In modern

systems, the interruption frequency can be up to 100 kHz. A PID feedback loop consists of three correcting terms, whose sum constitutes the Z-scanner position at a given time Z_t following the equation

$$Z_t = P\varepsilon_t + I\,\mathrm{d}t\sum_{i=0}^{t}\varepsilon_i + D\frac{\varepsilon_t - \varepsilon_{t-1}}{\mathrm{d}t} \tag{1.15}$$

where $t-1$ means $t-\mathrm{d}t$, ε_t is the error signal at time t (i.e., the difference between the measured value of the control parameter at time t and the set point value), and P, I, and D are the proportional, integral, and derivative gains, respectively. Currently, most AFMs employ a simplified version containing only two parameters P and I because differential control tends to introduce instabilities. Considering a PI feedback, one can evaluate the Z-scanner position at time $t-\mathrm{d}t$

$$Z_{t-1} = P\varepsilon_{t-1} + I\,\mathrm{d}t\sum_{i=0}^{t-1}\varepsilon_i \tag{1.16}$$

and after some manipulations

$$Z_t = Z_{t-1} + (P + I\,\mathrm{d}t)\varepsilon_t + P\varepsilon_{t-1} \tag{1.17}$$

This can be rewritten as

$$Z_t = Z_{t-1} + a\varepsilon_t + b\varepsilon_{t-1} \quad \text{with} \quad a = P + I\,\mathrm{d}t \quad \text{and} \quad b = -P \tag{1.18}$$

Proper feedback control requires fine tuning of the PI parameters. This is usually accomplished by the user by looking at the forward and backward scan signals and aiming to make them overlap. For low a and b values, the response of the system is very slow and the backward and forward profiles are very different. As one increases a and b, the response is faster, but if these parameters are too high, the system becomes unstable and the Z-piezoelectric oscillates at high frequency. In general, the working point is in-between these two situations and it is found following a trial-and error-procedure. In many commercial systems, there is an algorithm to optimize a and b.

1.7 Image Representation

The most outstanding feature of an AFM is its capability to produce three-dimensional, high-resolution images of a surface. A conventional AFM topography image is a surface function $z = f(x, y)$ that can be rendered in different ways. The most common rendering method consists of using a pseudo-color/gray scale map, in which each color/gray tone corresponds to a certain height (Figure 1.13). While this representation is quite intuitive, it does not provide a straightforward visual measurement of heights and distances. To quantify in-plane distances and heights, the usual procedure is to draw a profile line on the color map, resulting in a simple 2D representation (Figure 1.13b).

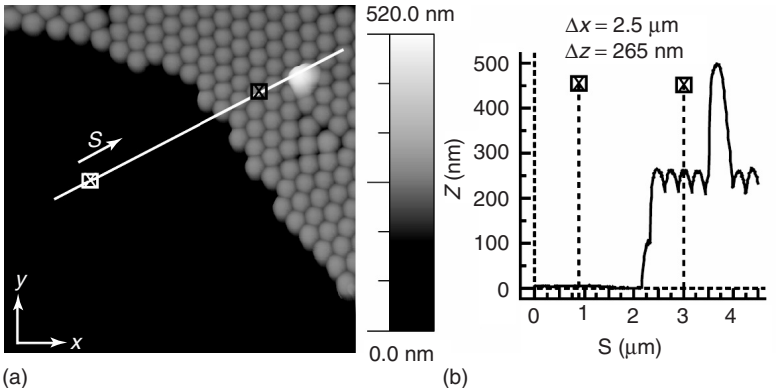

Figure 1.13 (a) AFM topography image of a single crystal made of polystyrene nanospheres. The height information is represented according to a color code included on the right of the image. (b) Height profile marked in the image.

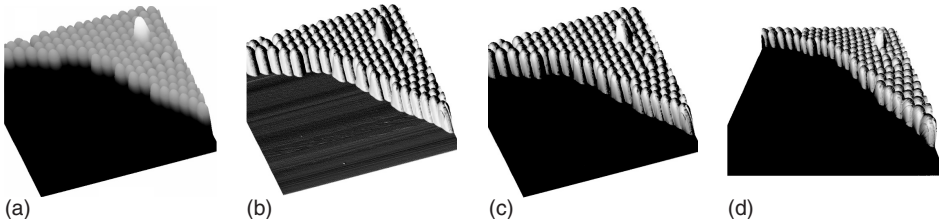

Figure 1.14 Three-dimensional rendering of the AFM topography shown in Figure 1.13. (a–c) Orthogonal views using different textures and shadows. (d) Change of the perspective of the projection.

A more intuitive representation is to render the image as a three-dimensional view, which can be displayed in several ways. For instance, the user can change the pseudo-color texture; apply shadows; change the angle of the illumination, the surface reflectivity, and the amount of ambient light; or change the view point of the image. All these different representation settings are used to enhance a certain detail of an image. Sometimes, 3D rendering must be done with caution because length scales of vertical and horizontal dimensions may be different. For instance, in the examples shown in Figure 1.14, the vertical height of the nanospheres is 265 nm, in contrast with the size of the image, which is 5 μm. Moreover, lateral and vertical dimensions may be distorted as a consequence of the projection used to display the data.

In addition to the surface representation methods described above, there are many filters that can be applied to an AFM image. Almost all AFM images are subjected to a filter known as *plane subtraction* because tip and sample planes are never parallel (Figure 1.15a). As a consequence, the angle between planes will

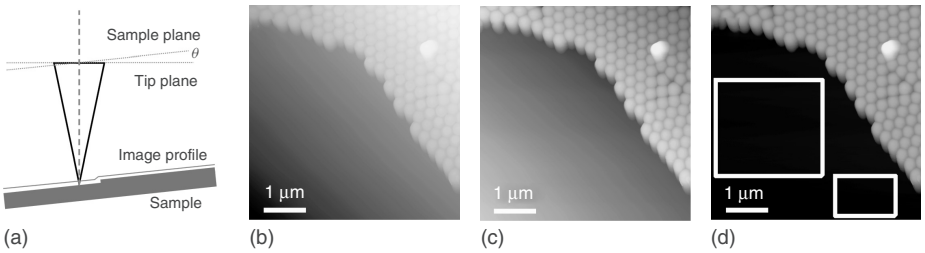

Figure 1.15 Plane subtraction filter. (a) Cartoon showing the angle difference between the tip plane and the sample plane. (b) Raw data showing a contrast caused by the surface tilt. (c) Data processed with a general plane subtraction filter. (d) Local plane subtraction filter. The squared areas are now used to calculate the plane that will be subtracted from the original image.

introduce a spurious height difference along the image (Figure 1.15b). This can be solved by calculating a general plane of the image and then subtracting it from the image raw data (Figure 1.15c). In general, this filter will flatten the image, but sometimes, the peculiarities of the data require some extra procedures. For instance, the data used to illustrate this example is clearly divided in two main planes: the basal surface and the plane given by the polystyrene nanospheres. A *local plane subtraction* considering only the data marked in squares in Figure 1.15d (basal plane) will give much better results, yielding the image shown in Figure 1.13.

Sometimes, raw data must be processed to reduce high-frequency noise or to enhance the edges of objects. This is done with low-pass or high-pass filters, respectively. High frequency noise can be removed by replacing the value of each image point by the average of next neighbors (nine data points). The *smoothing filter* is illustrated in Figure 1.16a,b with an image showing atomic periodicity of a highly oriented pyrolytic graphite (HOPG) surface. On the contrary, to enhance step edges of the graphite terraces in Figure 1.16c, the *derivative filtering* of the data along the *x*-direction should be applied (Figure 1.16d). Results similar to those shown in Figure 1.16 can be obtained in the reciprocal space using fast Fourier transform methods.

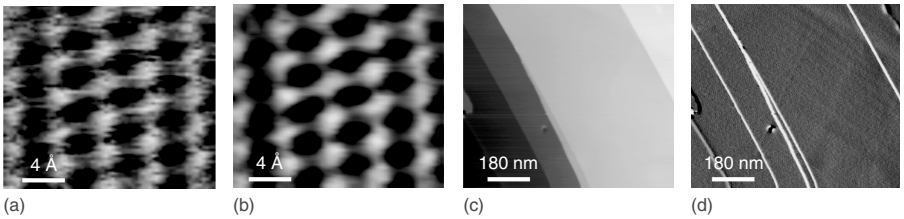

Figure 1.16 Smooth and derivative filters. (a) Raw data obtained showing the atomic periodicity of a HOPG surface. (b) Processed data of (a) with a low-pass filter (smoothed). (c) Atomically flat terraces of HOPG. (d) Derivative filter applied to (c) to enhance the step edges of the terraces.

A detailed description of data analysis for AFM is beyond the scope of this introduction. There are a number of powerful and flexible software applications allowing a variety of image filtering techniques, and some of them can be easily downloaded from the Internet. For instance, images shown in this section have been processed using WSxM [52], a freeware that can be downloaded from *www.nanotec.es*.

1.8
Artifacts and Resolution Limits

1.8.1
Artifacts Related to the Geometry of the Tip

The finite dimensions of the apex of an AFM tip produce images of objects that appear wider than they really are. This phenomenon known as *tip dilation* or convolution is particularly relevant when object dimensions are smaller that tip dimensions, and it affects the X and Y dimensions of an image (Figure 1.17). For instance, a typical AFM tip of 12 nm radius will produce an image of a DNA molecule (2 nm diameter) with a full width at half maximum (FWHM) of 10 nm. Some simple geometric models have been proposed to simulate the broadening

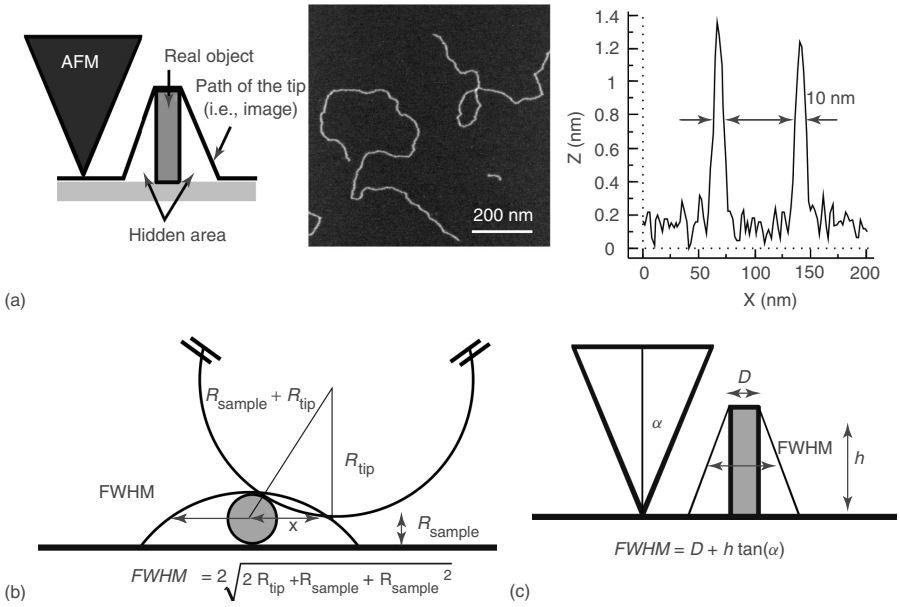

Figure 1.17 AFM broadening of objects. In the example shown in (a), the real object (a DNA molecule of around 2 nm diameter) appears five times wider because of the finite size of the AFM tip. This phenomenon is known as *tip dilation* or *convolution*. (b,c) Two models used to estimate tip dimensions from measurements of full width at half maximum considering a certain geometry of the tip and sample.

of the image by the tip. Figure 1.17b considers the tip as a spherical object of radius R_{tip} and a cylindrical object of radius R_{sample}. A simple calculation based on geometry yields a simple formula that allows an estimation of the radius of the tip from measurements of objects of known dimensions or geometry.

$$\mathrm{FWHM} = 2\sqrt{2R_{tip}R_{sample} + R_{sample}^2} \tag{1.19}$$

An alternative model considers a conical tip with an apex angle of 2α and a square object of dimensions $h \times D$ (Figure 1.17c). From geometry, one can derive the following equation:

$$\mathrm{FWHM} = \sqrt{D + h\tan(\alpha)} \tag{1.20}$$

A common artifact also related to the geometry of the tip is an effect known as *double tip*. The tip may possess two or more apexes, usually as a result of damage or contamination. This produces two or more copies of the image separated by a distance equal to the gap between the apexes (Figure 1.18). The appearance of a double-tip image depends on the size and height of the objects subjected to scan. Sometimes, the secondary apex is tens of nanometers above the main imaging apex and therefore, it only becomes obvious when imaging objects of that height. In general, when imaging small objects such as DNA or proteins (1–2 nm of height), no double-tip effect appears, but rather, broadening and loss of resolution due to blunting of the tip or contamination occurs.

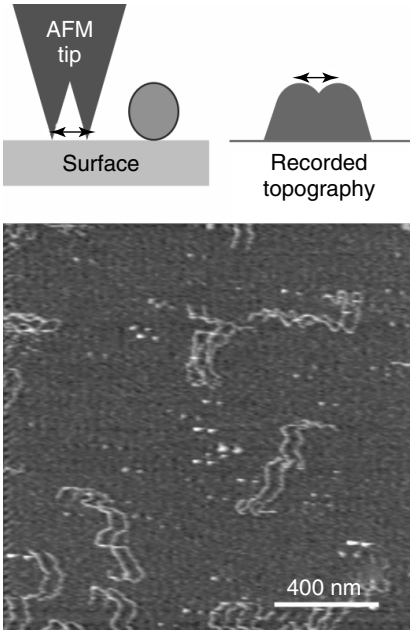

Figure 1.18 Double-tip effect.

1.8.2
Artifacts Related to the Feedback Loop

One of the most common sources for artifacts in AFM images is the feedback. The magnitude of the proportional and integral parameter (Section 1.6) depends on many factors, which include the type of piezoelectric scanner, the particular type of cantilever used, the state of the tip, the vibration level of the building, and so on. While some modern systems include software utilities that help tuning the feedback, in many other cases, the feedback must be adjusted by the user. The number of possible artifacts is too broad to be described here, but there are two kinds that are particularly common. Correct adjustment of *a* and *b* (Section 1.6) leads to similar images regardless of the direction of the scan used for acquisition (Figure 1.19a,b). If *a* and *b* are too small, the response of the system is very slow, and that results in asymmetric images as shown in Figure 1.19c,d. The effect of a slow feedback is obvious when recording the backward and forward profiles because surface protrusions are elongated along the scan direction. On the other hand, if *a* and *b* are too high, the system becomes unstable and a high-frequency oscillation is observed in the image (Figure 1.19e,f). Often, this high-frequency oscillation, present in both forward and backward profile directions, can be wrongly attributed to real surface features.

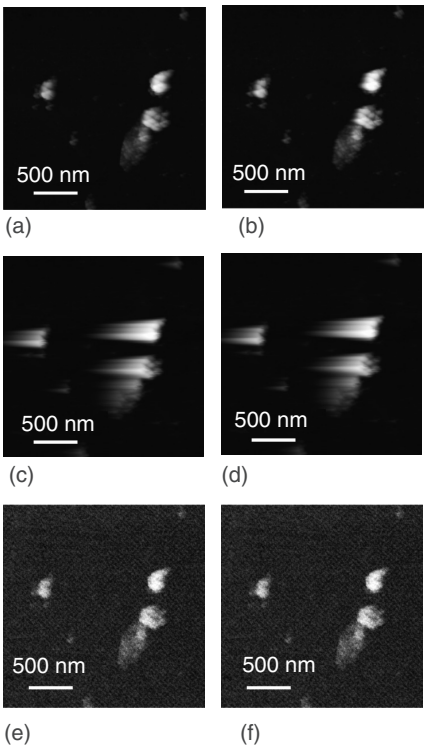

Figure 1.19 Artifacts related to the feedback loop. Left-column images were acquired from left to right (forward direction) and right-column images were acquired from right to left (backward direction). (a,b) represent examples of correct use of feedback parameters, (c,d) are examples of a too low feedback, and (e,f) of a too high feedback.

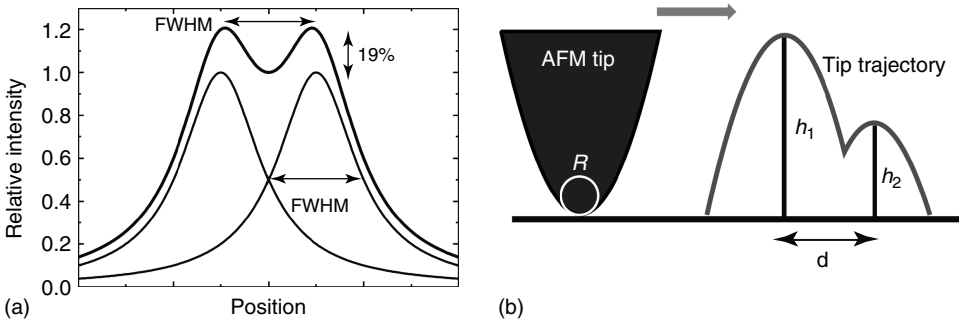

Figure 1.20 (a) Resolution criterion for a Fabry–Perot interferometer: the peaks are separated by one FWHM of each. (b) Spatial resolution in AFM. Two objects need a minimum distance d to be resolved. This distance d is dependent on the dimensions and shape of the tip and on the relative height of the objects.

1.8.3 Resolution Limits

Spatial resolution in AFM is a complex subject to address because AFM imaging is a three-dimensional imaging technique and tip convolution is not linear. Lateral resolution is usually defined by the ability to distinguish two separate points on an image. In radiation-based microscopies, spatial resolution is limited by diffraction, but in AFM, lateral resolution is defined by two factors: the pixel size of the image and the radius of the tip. Typical images in air or in liquids have a pixel size of 1–2 nm (500 nm at 512 pixels). For this reason, large images are in general limited by the pixel size.

In the microscopy community, one of the criteria used to define resolution was given by Fabry and Perot: two peaks of equal intensity are resolved if they are at least separated by FWHM of each. The dip height of the combined profile is nearly 0.81 times the maximum height [53] (Figure 1.20a). Similarly, in AFM we may ask: what is the minimum distance we can resolve in a two-point-like object configuration? (Figure 1.20b)

Considering that each object produces an image of the parabolic AFM tip, we can formulate an equation for the image of an object of height h_1

$$y_1 = h_1 - \frac{x^2}{2R} \tag{1.21}$$

For $y_1 = h_2$ we obtain

$$\Delta h = h_1 - h_2 = \frac{x^2}{2R} \tag{1.22}$$

Therefore the distance between these two points must be

$$d \geq \sqrt{2R\Delta h} \tag{1.23}$$

This explains why two objects closely spaced and of similar heights can be distinguished provided the tip is sharp enough, in contrast with radiation-based microscopic techniques, which are limited by the wavelength of the light. This also means that true atomic resolution can be achieved with AFM if interaction between the tip and sample is done only through the atom at the very end of the tip [54]. In contact mode and on hard surfaces, true atomic resolution was achieved in 1993 by Ohnesorge and Binnig [55]. Recently, using FM-AFM also true atomic resolution has been achieved in liquids [41]. For biological samples in liquids, the ultimate resolution is achieved on crystal-like arrays of membrane proteins. In 1995, Muller *et al.* [28] imaged the purple membrane at subnanometer resolution.

Acknowledgments

Fernando Moreno-Herrero acknowledges support from a starting grant from the European Research Council (Grant 206117) and by a grant from the Spanish Ministry of Science and Innovation (Grant FIS2008-0025). Julio Gomez-Herrero acknowledges support from the Spanish Ministry of Science and Innovation (Grants MAT2010-20843-C02-01, CSD2010_00024) and from Comunidad de Madrid (Grant S2009/MAT-1467).

References

1. Binnig, G. and Rohrer, H. (1982) Scanning tunneling microscopy. *Helv. Phys. Acta.*, **55**, 726–735.
2. Binnig, G., Quate, C.F., and Gerber, C. (1986) Atomic force microscope. *Phys. Rev. Lett.*, **56**, 930–933.
3. Giessibl, F.J. and Quate, C.F. (2006) Exploring the nanoworld with atomic force microscopy. *Phys. Today*, **59**, 44–50.
4. Bustamante, C. and Keller, D. (1995) Scanning force microscopy in biology. *Phys. Today*, **48**, 32–38.
5. Bustamante, C., Rivetti, C., and Keller, D.J. (1997) Scanning force microscopy under aqueous solutions. *Curr. Opin. Struct. Biol.*, **7**, 709–716.
6. Binnig, G. and Smith, D.P.E. (1986) Single-tube 3-dimensional scanner for scanning tunneling microscopy. *Rev. Sci. Instrum.*, **57**, 1688–1689.
7. Rubio, G., Agrait, N., and Vieira, S. (1996) Atomic-sized metallic contacts: mechanical properties and electronic transport. *Phys. Rev. Lett.*, **76**, 2302–2305.
8. Cleveland, J.P., Manne, S., Bocek, D., and Hansma, P.K. (1993) A non-destructive method for determining the spring constant of cantilevers for scanning force microscopy. *Rev. Sci. Instrum.*, **64**, 403–405.
9. Sader, J.E., Larson, I., Mulvaney, P., and White, L.R. (1995) Method for calibration of atomic force cantilevers. *Rev. Sci. Instrum.*, **66**, 3789–3798.
10. Seder, J.E., Chon, J.W.M., and Mulvaney, P. (1999) Calibration of rectangular atomic force microscope cantilevers. *Rev. Sci. Instrum.*, **70**(10), 3967–3969.
11. Green, C.P., Lioe, H., Cleveland, J.P., Proksch, R., Mulvaney, P., and Sader, J.E. (2004) Normal and torsional spring constants of atomic force microscope cantilevers. *Rev. Sci. Instrum.*, **75**, 1988–1996.
12. Israelachvili, J. (1991) *Intermolecular and Surface Forces*, Academic Press, London.
13. Sader, J.E. (1998) Frequency response of cantilever beams immersed in viscous fluids with applications to the atomic force microscope. *J. Appl. Phys.*, **84**, 64.
14. García, R. and Pérez, R. (2002) Dynamic atomic force microscopy methods. *Surf. Sci. Rep.*, **47**, 197–301.

15. French, A.P. (1971) *Vibrations and Waves*, W.W. Norton and Co., New York.
16. Tamayo, J., Humphris, A.D.L., Owen, R.J., and Miles, M.J. (2001) High-Q dynamic force microscopy in Liquids and its application to living cells. *Biophys. J.*, **81**, 526–537.
17. Moreno-Herrero, F., Colchero, J., Gomez-Herrero, J., and Baro, A.M. (2004) Atomic force microscopy contact, tapping, and jumping modes for imaging biological samples in liquids. *Phys. Rev. E. Stat. Nonlin. Soft. Matter Phys.*, **69**, 031915.
18. Cleveland, J.P., Anczykowski, B., Schmid, A.E., and Elings, V.B. (1998) Energy dissipation in tapping-mode atomic force microscopy. *Appl. Phys. Lett.*, **72**, 2613–1615.
19. Xu, X., Carrasco, C., de Pablo, P.J., Gomez-Herrero, J., and Raman, A. (2008) Unmasking imaging forces on soft biological samples in liquids when using dynamic atomic force microscopy: a case study on viral capsids. *Biophys. J.*, **95**, 2520–2528.
20. Moreno-Herrero, F., de Jager, M., Dekker, N.H., Kanaar, R., Wyman, C., and Dekker, C. (2005) Mesoscale conformational changes in the DNA-repair complex Rad50/Mre11/Nbs1 upon binding DNA. *Nature*, **437**, 440–443.
21. Manalis, S.R., Minne, C.S., and Quate, C.F. (1996) Atomic force microscopy for high speed imaging using cantilevers with an integrated actuator and sensor. *Appl. Phys. Lett.*, **68** (6), 871–873.
22. Rogers, B., York, D., Whisman, N., Jones, M., Murray, K., Adams, J.D., Sulchek, T., and Minne, C. (2002) Tapping mode atomic force microscopy in liquid with an insulated piezoelectric microactuator. *Rev. Sci. Instrum.*, **73**, 3242–3244.
23. Giessibl, F.J. (1995) Atomic resolution of the silicon(111)-7x7 surface by atomic force microscopy. *Science*, **267**, 68–71.
24. Meyer, G. and Amer, N.M. (1988) Novel optical approach to atomic force microscopy. *Appl. Phys. Lett.*, **53**, 1045.
25. Alexander, S., Hellemans, L., Marti, O., Schneir, J., Elings, V., Hansma, P.K., Longmire, M., and Gurley, G. (1989) An atomic-resolution atomic-force microscope implemented using an optical lever. *J. Appl. Phys.*, **65**, 164.
26. Moreno-Herrero, F., de Pablo, P.J., Colchero, J., Gómez-Herrero, J., and Baró, A.M. (2000) The role of shear forces in scanning force microscopy: a comparison between the jumping mode and tapping mode. *Surf. Sci.*, **453**, 152–158.
27. Sarid, D. (1991) *Scanning Force Microscopy with Applications to Electric, Magnetic, and Atomic Forces*, Oxford University Press, Oxford.
28. Muller, D.J., Schabert, F.A., Büldt, G., and Engel, A. (1995) Imaging purple membranes in aqueous solutions at sub-nanometer resolution by atomic force microscopy. *Biophys. J.*, **68**, 1681–1686.
29. Mou, J.X., Yang, J., and Shao, Z.F. (1996) High resolution surface of E.coli GroES oligomer by atomic force microscopy. *FEBS. Lett.*, **381**, 161–164.
30. de Pablo, P.J., Colchero, J., Gómez-Herrero, J., and Baro, A.M. (1998) Jumping mode scanning force microscopy. *Appl. Phys. Lett.*, **73**, 3300–3302.
31. Rosa-Zeise, A., Weilandt, E., Hild, S., and Marti, O. (1997) The simultaneous measurement of elastic, electrostatic and adhesive properties by scanning force microscopy: pulsed-force mode operation. *Meas. Sci. Technol.*, **8**, 1333–1338.
32. Moreno-Herrero, F., de Pablo, P.J., Fernández-Sánchez, R., Colchero, J., Gómez-Herrero, J., and Baró, A.M. (2002) Scanning force microscopy jumping and tapping modes in liquids. *Appl. Phys. Lett.*, **81**, 2620–2623.
33. Carrasco, C., Carreira, A., Schaap, I.A., Serena, P.A., Gomez-Herrero, J., Mateu, M.G., and de Pablo, P.J. (2006) DNA-mediated anisotropic mechanical reinforcement of a virus. *Proc. Natl. Acad. Sci. U.S.A.*, **103**, 13706–13711.
34. Schaap, I.A., Carrasco, C., de Pablo, P.J., MacKintosh, F.C., and Schmidt, C.F. (2006) Elastic response, buckling, and instability of microtubules under radial indentation. *Biophys. J.*, **91**, 1521–1531.
35. Rief, M., Gautel, M., Oesterhelt, F., Fernandez, J.M., and Gaub, H.E. (1997)

Reversible unfolding of individual titin immunoglobulin domains by AFM. *Science*, **276**, 1109–1112.
36. Martin, Y., Williams, C.C., and Wickramasinghe, H.K. (1987) Atomic force microscopy mapping and profiling on a sub 100-A scale. *J. Appl. Phys.*, **61**, 4723–4729.
37. Zhong, Q., Inniss, D., Kjoller, K., and Elings, V.B. (1993) Fractured polymer/silica fiber surface studied by tapping mode atomic force microscopy. *Surf. Sci. Lett.*, **290**, L688–L692.
38. Putman, A.J., van der Werf, K.O., de Grooth, B., van Hulst, N.F., and Greve, J. (1994) Tapping mode atomic force microscopy in liquid. *Appl. Phys. Lett.*, **72**, 2454–2456.
39. Albrecht, T.R., Grutter, P., Horne, D., and Rugar, D. (1991) Frequency modulation detection using high-Q cantilevers for enhanced force microscope sensitivity. *J. Appl. Phys.*, **69**, 668–673.
40. Higgins, M.J., Riener, C.K., Uchihashi, T., Sader, J.E., McKendry, R., and Jarvis, S.P. (2005) Frequency modulation atomic force microscopy: a dynamic measurement technique for biological systems. *Nanotechnology*, **16**, s85.
41. Fukuma, T. and Jarvis, S.P. (2006) Development of liquid-environment frequency modulation atomic force microscope with low noise deflection sensor for cantilevers of various dimensions. *Rev. Sci. Instrum.*, **77**, 043701–043708.
42. Fukuma, T., Ueda, Y., Yoshioka, S., and Asakawa, H. (2010) Atomic-scale distribution of water molecules at the mica-water interface visualized by three-dimensional scanning force microscopy. *Phys. Rev. Lett.*, **104**, 016101-1–016101-4.
43. Hansma, P.K., Cleveland, J.P., Radmacher, M., Walters, D.A., Hillner, P.E., Bezanilla, M., Fritz, M., Vie, D., Hansma, H.G., Prater, C.B. *et al.* (1994) Tapping mode atomic force microscopy in liquids. *Appl. Phys. Lett.*, **64**, 1738–1740.
44. Florin, E.-L., Radmacher, M., Fleck, B., and Gaub, H.E. (1994) Atomic force microscope with magnetic force modulation. *Rev. Sci. Instrum.*, **65**, 639.
45. O'Shea, S.J., Welland, M.E., and Pethica, J.B. (1994) Atomic force microscopy of local compliance at solid-liquid interfaces. *Chem. Phys. Lett.*, **223**, 336–340.
46. Han, W., Lindsay, S.M., and Jing, T. (1996) A magnetically driven oscillating probe microscope for operation in liquids. *Appl. Phys. Lett.*, **69**, 4111–4113.
47. Umeda, K., Oyabu, N., Kobayashi, K., Hirata, Y., Matsushige, K., and Yamada, H. (2010) High-resolution frequency-modulation atomic force microscopy in liquids using electrostatic excitation method. *Appl. Phys. Express*, **3**, 065205.
48. Carrasco, C., Ares, P., de Pablo, P.J., and Gomez-Herrero, J. (2008) Cutting down the forest of peaks in acoustic dynamic atomic force microscopy in liquid. *Rev. Sci. Instrum.*, **79**, 126106.
49. Asakawa, H. and Fukuma, T. (2009) Spurious-free cantilever excitation in liquid by piezoactuator with flexure drive mechanism. *Rev. Sci. Instrum.*, **80**, 103703–103705.
50. Stahl, S.W., Puchner, E.M., and Gaub, H.E. (2009) Photothermal cantilever actuation for fast single-molecule force spectroscopy. *Rev. Sci. Instrum.*, **80**, 073702.
51. Piner, R. and Reifenberger, R. (1989) Computer control of the tunel barrier width for the scanning tunneling microscope. *Rev. Sci. Instrum.*, **60**, 3123.
52. Horcas, I., Fernandez, R., Gomez-Rodriguez, J.M., Colchero, J., Gomez-Herrero, J., and Baro, A.M. (2007) WSXM: a software for scanning probe microscopy and a tool for nanotechnology. *Rev. Sci. Instrum.*, **78**, 013705.
53. Sharma, K.K. (2006) *Optics: Principles and Applications*, Elsevier, Oxford.
54. Morita, S., Wiesendanger, R., and Meyer, E. (2002) *Noncontact Atomic Force Microscopy*, Springer, Berlin.
55. Ohnesorge, F. and Binnig, G. (1993) True atomic resolution by atomic force microscopy through repulsive and attractive forces. *Science*, **260**, 1451.